Raman and x-ray study of $La_{1-x}Nd_xGaO_3$ $(0 \leqslant x \leqslant 1)$ perovskite solid solutions

1998 J. Phys.: Condens. Matter 10 11687

(http://iopscience.iop.org/0953-8984/10/50/008)

J. Phys.: Condens. Matter **10** (1998) 11687–11702. Printed in the UK PII: S0953-8984(98)94268-0

Raman and x-ray study of $La_{1-x}Nd_xGaO_3$ ($0 \leqslant x \leqslant 1$) perovskite solid solutions

M L Sanjuán, V M Orera, R I Merino and J Blasco

Instituto de Ciencia de Materiales de Aragón (Universidad de Zaragoza—CSIC), Facultad de Ciencias, Universidad de Zaragoza, 50009 Zaragoza, Spain

Received 13 May 1998, in final form 7 October 1998

Abstract. La and Nd gallates are currently being used as substrate materials for high temperature superconductor thin film deposition. In this work we have synthesized and characterized by means of XRD and Raman spectroscopy solid solutions of the type $La_{1-x}Nd_xGaO_3$ ($0 \leqslant x \leqslant 1$). Polarized Raman study of $LaGaO_3$ and $NdGaO_3$ single crystals is also performed. Our results confirm the *Pbnm* space group for both La and Nd perovskites at room temperature and the centrosymmetric $R\bar{3}c$ for $LaGaO_3$ in the high temperature phase. The orthorhombic to rhombohedral first order phase transition ($T_c = 423$ K in $LaGaO_3$) is studied as a function of Nd substitution. T_c increases quadratically with x for $x \leqslant 0.14$. Beyond $x = 0.17$ the phase transition, if present, is above the limit of our experimental setup (870 K). The detection of a soft A_{1g} mode in the rhombohedral phase is interpreted as due to the existence of a virtual second order transition to cubic symmetry at high temperature, analogous to that observed in rare earth aluminates.

1. Introduction

Since the discovery of high temperature superconductivity (HTS) a great interest in HTS thin film research has arisen owing to their potential applications in electronic devices. High quality HTS thin film preparation requires a careful substrate selection to achieve a good epitaxial film growth. Oxides with perovskite structure have been extensively explored as they comply with most of the requirements for appropriate HTS substrates, such as good lattice match, coincidence of ion sites, similar crystal structures and good surface and structural quality [1].

In particular $LaGaO_3$ and $NdGaO_3$ were proposed as potential substrate materials due to their quite good lattice and thermal expansion match with HTS materials such as $YBa_2Cu_3O_7$, and their low dielectric constant ($\varepsilon \approx 20$) [1]. However, the existence of a structural phase transition at about 150 °C in $LaGaO_3$, and the presence of Nd^{3+} magnetic ions, in $NdGaO_3$, render difficult the use of these materials as substrates for some devices (see [1] and references therein for a review of their general properties).

In spite of the numerous studies performed, the crystal structure of these materials is still a matter of some controversy. In a previous work based on neutron powder diffraction, Marti *et al* [2] proposed for the room temperature (RT) structure of $LaGaO_3$ the centrosymmetric orthorhombic (OR) group *Pbnm* (D_{2h}^{16}) and the non-centrosymmetric group $Pbn2_1$ (C_{2v}^{9}) for $NdGaO_3$. They also proposed a non-centrosymmetric structure, with space group $R3c$ (C_{3v}^{6}), for the high temperature rhombohedral (RH) phase of $LaGaO_3$. However, in later work [3] they refined their neutron data and found similar reliability factors using the centrosymmetric groups *Pbnm* for $NdGaO_3$ at RT, and $R\bar{3}c$ (D_{3d}^{6}) for $LaGaO_3$ above T_c.

0953-8984/98/5011687+16$19.50

From the point of view of their structure gallates can be compared with other oxide systems, in particular with rare earth aluminates. At RT the aluminates of the lighter rare earths La, Pr and Nd are trigonal (space group $R\bar{3}c$) [4, 5] while for the heavier, from Sm to Yb, and also for Y, they are OR ($Pbnm$) [5, 6]. Above RT trigonal aluminates undergo a second order phase transition to cubic structure ($Pm3m$) whereas OR aluminates such as $SmAlO_3$ and $EuAlO_3$ suffer a previous first order transition into $R\bar{3}c$ phase [7–9]. A depiction of cubic, OR and RH perovskite structures can be found in [6].

The low symmetry phases of ABX_3 perovskites may often be understood as a freezing in of zone boundary modes of the cubic structure, associated with tilts of the BX_6 octahedra [10]. Thus, the OR $Pbnm$ structure results from two equivalent anti-phase tilts around the x and y cubic axes and an in-phase tilt around the z axis ($a^-a^-c^+$ in Glazer's notation), together with displacement of cation A along x, y OR directions. The high temperature RH phase of $LaGaO_3$, in contrast, arises from equal anti-phase rotations around all three cubic axes ($a^-a^-a^-$). No shifts of A and B cations occur in this case.

In the present work we apply Raman spectroscopy to the $La_{1-x}Nd_xGaO_3$ system, focusing in the mode attribution across the series and their temperature evolution. Previous Raman studies go back to the early work of Saine *et al* [11] in polycrystalline samples of the end compounds. Their results are revisited here using both ceramic and single crystal samples.

We have prepared solid solutions with $0 \leqslant x \leqslant 1$ and determined their structure from x-ray diffraction patterns. The results of our structural analysis are given in section 3. In section 4 we present experimental Raman results and their interpretation, first at a fixed temperature (RT for the OR phase of either pure or doped compounds, above T_c for the RH phase of $LaGaO_3$), and then as a function of temperature. Finally, in section 5 we comment on the effect of rare-earth substitution in the OR $\rightarrow$ RH first order transition, particularly on the disappearance of the transition as the Nd content is increased. The interest of our results from a technological point of view is briefly discussed in the conclusions.

2. Experimental details

The $NdGaO_3$ and $LaGaO_3$ single crystals used in this study were grown by the Bridgman and flame fusion method, respectively. The $NdGaO_3$ sample was a large, twin free single crystal of excellent optical and mechanical quality. $LaGaO_3$ single crystals were small ($\approx$1 mm^3) and presented twinning along pseudocubic crystallographic axes. They were doped with $\approx$1 at.% of Nd for spectroscopic measurements not included in this work.

The crystals were oriented using the back-reflection Laue method and cut and polished to allow polarized Raman measurements along the principal crystallographic directions. $La_{1-x}Nd_xGaO_3$ samples were prepared using the solid state reaction method for ceramic synthesis. La_2O_3, Ga_2O_3 and Nd_2O_3 powders were previously calcinated at 850 °C. The mixture in the appropriate ratio of the components was milled for homogenization, pelletized and sintered in air at 1450 °C for 12 h. The milling and sintering process was done twice to obtain a good sample homogeneity.

X-ray diffraction patterns were obtained at room temperature using a Rigaku diffractometer with a rotating anode (D-maxB system). The device was operated at 100 mA and 40 kV with a Cu anode. A graphite monochromator was used to select Cu $K\alpha_{1,2}$ radiation. Data were collected from 20 up to 120° in 2θ with a step size of 0.02° and counting time of 8 s/step. The structures of $La_{1-x}Nd_xGaO_3$ compounds were refined by the full-pattern Rietveld method using the FULLPROF program [12].

The phase transition was studied by differential scanning calorimetry (DSC) with a DSC 7 Perkin–Elmer instrument.

The Raman spectra were measured at temperatures between 300 and 860 K in backscattering geometry, in a Dilor *XY* spectrometer with diode array multichannel detector and a $\times 50$ microscope objective lens. Measurements above RT were performed in a Linkam TP91 thermostage with a temperature stability of ± 0.5 K. To avoid Nd^{3+} light emissions, different lines of a Coherent Ar^+ laser were used. The light power at the sample was of the order of 50 mW and the spectral resolution better than 3 cm^{-1}.

3. Structural analysis

$LaGaO_3$ and $NdGaO_3$ have the orthorhombic $GdFeO_3$ structure with *Pbnm* space group at RT in agreement with recent results reported [3]. The same structure is found in the whole $La_{1-x}Nd_xGaO_3$ series without any additional diffraction peaks, indicating a perfect solid solution. In this structure, Ga^{3+} ions are fixed at the 4(b) ($\bar{1}$) position: $(1/2, 0, 0)$. The rare earth atoms and the apical oxygen of the anion octahedra, O(1), occupy the 4(c) (..m) position: $(x, y, 1/4)$. Finally, equatorial oxygens, O(2), are located at 8(d) (1): (x, y, z). Figure 1 shows the observed x-ray diffraction pattern for $NdGaO_3$ together with the best fit obtained.

The refined cell parameters, atomic positions, isotropic temperature factors and the reliability factors are summarized in table 1. We also give the main interatomic distances and angles calculated from the refined atomic positions. From these data we see that the unit cell volume decreases along the series with increasing Nd content in agreement with the lanthanide contraction. The small Nd^{3+} ion leads to an increase of the orthorhombic distortion as can be inferred from the decrease of the Ga–O–Ga angle. The consequent displacements of oxygen and rare earth atoms mainly produce a decrease of *a* and *c* unit cell parameters while the *b* parameter remains practically unchanged in the whole series. Furthermore, $a > b$ for $LaGaO_3$ while $a < b$ for $NdGaO_3$.

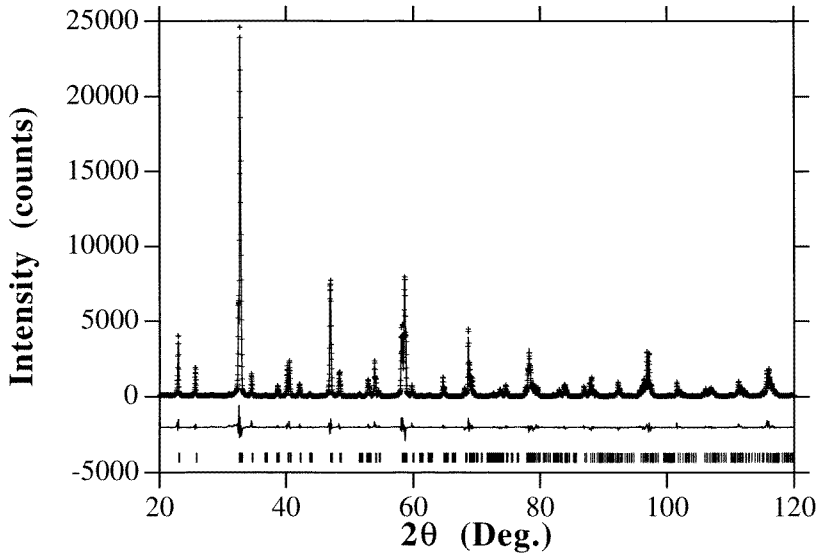

Figure 1. XRD pattern of an $NdGaO_3$ polycrystalline sample. Crosses represent experimental points and continuous line the fit to *Pbnm* space group with parameters given in the text. The lower curve is the difference between the experiment and the fit.

Table 1. Structural parameters obtained for $La_{1-x}Nd_xGaO_3$ from XRD at room temperature. Refined lattice parameters, fractional coordinates, isotropic temperature factors, reliability factors, interatomic distances (Å) in Ga–O and R–O (R: La, Nd) polyhedra, and angles between neighbouring octahedra (°).

	$x = 0$	$x = 0.1$	$x = 0.2$	$x = 0.4$	$x = 0.6$	$x = 0.75$	$x = 1$
a (Å)	5.5217(1)	5.5116(1)	5.5006(1)	5.4845(3)	5.4641(1)	5.4495(2)	5.4264(1)
b (Å)	5.4893(1)	5.4886(1)	5.4878(1)	5.4878(2)	5.4884(1)	5.4874(1)	5.4958(1)
c (Å)	7.7701(1)	7.7672(1)	7.7630(1)	7.7554(4)	7.7428(2)	7.7355(2)	7.7060(1)
V (Å^3)	235.5	235.0	234.3	233.4	232.2	231.3	229.81
R: x	−0.0043(2)	−0.0036(3)	−0.0045(3)	−0.0073(3)	−0.0072(2)	−0.0085(2)	−0.0091(2)
y	−0.0171(1)	−0.0201(1)	−0.0231(1)	−0.0289(1)	−0.0328(1)	−0.0360(1)	−0.0416(1)
B (Å^2)	0.46(2)	0.65(1)	0.87(2)	0.72(2)	0.39(1)	0.46(2)	0.17(2)
Ga: B (Å^2)	0.48(2)	0.65(2)	0.86(2)	0.95(2)	0.36(2)	0.53(2)	0.30(2)
O1: x	0.0654(20)	0.0626(19)	0.0689(26)	0.0712(26)	0.0831(23)	0.0837(25)	0.0850(17)
y	0.5039(16)	0.4981(12)	0.5074(15)	0.5285(19)	0.5144(13)	0.5136(16)	0.5211(15)
B (Å^2)	0.85(23)	0.05(21)	0.65(31)	0.91(33)	0.72(24)	0.96(26)	0.61(10)
O2: x	0.7704(19)	0.7720(17)	0.7770(19)	0.7827(21)	0.7921(13)	0.7860(13)	0.7860(13)
y	0.2275(18)	0.2253(17)	0.2256(21)	0.2167(21)	0.2123(13)	0.2137(15)	0.2059(12)
z	0.0378(10)	0.0391(19)	0.0405(28)	0.0364(14)	0.0375(12)	0.0340(10)	0.0436(9)
B (Å^2)	0.80(12)	0.83(15)	0.96(18)	0.92(19)	0.44(14)	0.08(18)	0.12(10)
R_p (%)	8.9	9.6	8.5	8.2	8.3	8.8	9.5
R_{wp} (%)	12.1	13.0	11.5	11.2	11.9	12.0	13.1
R_B (%)	6.9	6.7	4.6	5.1	5.1	3.8	5.9
Ga–O1: (×2)	1.976(2)	1.972(2)	1.978(3)	1.980(3)	1.989(3)	1.988(3)	1.983(2)
Ga–O2: (×2)	1.968(10)	1.967(10)	1.988(11)	1.974(13)	1.983(8)	1.968(7)	1.949(7)
(×2)	1.983(10)	1.986(10)	1.967(11)	1.979(13)	1.973(8)	1.974(8)	2.018(7)
⟨Ga–O⟩:	1.976	1.975	1.978	1.978	1.981	1.977	1.983
Ga–O1–Ga:							
(×2)	158.9(4)	159.8(4)	157.8(5)	156.5(6)	153.2(5)	153.2(5)	152.3(4)
Ga–O2-Ga:							
(×4)	160.3(17)	159.4(12)	158.3(20)	157.8(24)	156.3(13)	157.5(12)	153.3(9)
R–O1: (×1)	2.426(11)	2.433(11)	2.402(14)	2.406(16)	2.332(14)	2.331(14)	2.326(10)
(×1)	2.657(9)	2.669(7)	2.608(8)	2.521(10)	2.534(9)	2.522(9)	2.456(8)
(×1)	2.886(9)	2.867(7)	2.939(14)	3.035(10)	3.043(9)	3.057(9)	3.133(8)
(×1)	3.100(11)	3.083(11)	3.109(14)	3.104(16)	3.157(14)	3.146(14)	3.143(10)
R–O2: (×2)	2.464(9)	2.455(9)	2.440(11)	2.426(13)	2.409(9)	2.434(8)	2.369(7)
(×2)	2.616(9)	2.612(9)	2.606(11)	2.641(13)	2.642(9)	2.639(8)	2.560(7)
(×2)	2.829(9)	2.818(9)	2.808(10)	2.741(12)	2.718(9)	2.692(8)	2.720(7)
(×2)	3.135(9)	3.157(9)	3.186(11)	3.225(12)	3.257(9)	3.245(8)	3.329(7)

From the values given in table 1 we see that GaO_6 octahedra are nearly perfect. The average Ga–O distance fairly well agrees with that expected from theoretical ionic radii, 1.97 Å [13]. Small differences between Ga–O(2) distances (equatorial oxygens) seem to exist in $NdGaO_3$. This can be understood in the frame of the bond valence model [14]. It is well known that a slight distortion in a coordination sphere leaving constant the average distance leads to an increase of the valence state in the central atom. The slight deformation of the GaO_6 octahedron preserves the oxidation state for the Ga^{3+} ion in spite of increasing the acid character of the rare earth ion (Nd^{3+} is smaller than La^{3+}).

The effective oxygen coordination for rare earth ions is lower than in the ideal cubic case (12) because rare earth–oxygen bond distances are not long enough to allow non-tilted octahedra. La is basically nine coordinated in $LaGaO_3$ while Nd is eight coordinated in $NdGaO_3$.

4. Raman spectra and interpretation

4.1. Pure compounds, OR phase

At RT both $LaGaO_3$ and $NdGaO_3$ present the *Pbnm* space group, with four formula units per unit cell ($Z = 4$). Then, 60 lattice modes are expected at each phonon wave vector which decompose in the following way at the zone centre:

$$7A_g + 7B_{1g} + 5B_{2g} + 5B_{3g} + 8A_u + 8B_{1u} + 10B_{2u} + 10B_{3u}$$

resulting in 24 Raman active modes, 25 infrared active modes, eight inactive A_u and three ($B_{1u} + B_{2u} + B_{3u}$) acoustic translational modes [15]. We shall use two different sets of measurements in order to obtain a complete symmetry assignment: along OR axes (x, y, z), that are parallel to OR directions $\boldsymbol{a}$, $\boldsymbol{b}$, $\boldsymbol{c}$, and along pseudocubic axes (x', y', z), that can be obtained from the OR ones through a 45° rotation about the common z axis. Referred to the OR axes, the Raman tensors pertaining to OR symmetry are

$$\underset{A_{1g}}{\begin{bmatrix} a & & \\ & b & \\ & & c \end{bmatrix}}, \underset{B_{1g}}{\begin{bmatrix} & d & \\ d & & \\ & & \end{bmatrix}}, \underset{B_{2g}}{\begin{bmatrix} & & e \\ & & \\ e & & \end{bmatrix}}, \underset{B_{3g}}{\begin{bmatrix} & & \\ & & f \\ & f & \end{bmatrix}}$$

and referred to pseudocubic axes (x', y', z)

$$\underset{A_{1g}}{\frac{1}{2}\begin{bmatrix} a+b & -a+b & \\ -a+b & a+b & \\ & & 2c \end{bmatrix}}, \underset{B_{1g}}{\begin{bmatrix} d & & \\ & -d & \\ & & \end{bmatrix}}, \underset{B_{2g}}{\frac{1}{\sqrt{2}}\begin{bmatrix} & & e \\ & & -e \\ e & -e & \end{bmatrix}}, \underset{B_{3g}}{\frac{1}{\sqrt{2}}\begin{bmatrix} & & f \\ & & f \\ f & f & \end{bmatrix}}.$$

We shall denote by $\alpha\beta$ the experimental configuration used in polarization measurements, where α and β stand for the incoming and outgoing electric field polarization, respectively. For $NdGaO_3$ single crystals we have measured xx, yy, zz, xy, xz, yz, $x'x'$, $x'y'$ and $y'y'$ spectra.

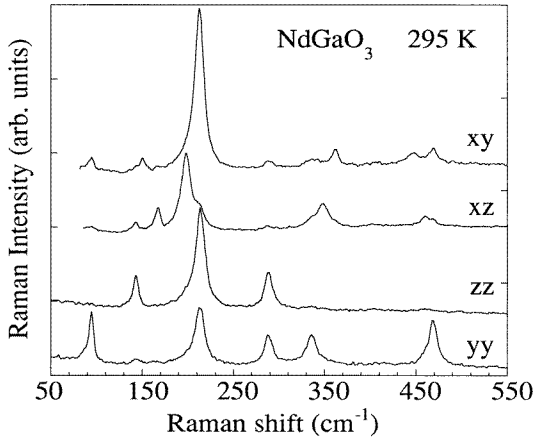

Figure 2. RT Raman spectra of an $NdGaO_3$ single crystal taken with $\lambda = 488$ nm in the polarization configurations indicated, where x, y, z stand for orthorhombic axes. The 488 nm laser line was chosen to avoid Nd emission bands which are seen in the phonon energy region when exciting with lower energy lines.

In figure 2 we show phonon Raman spectra of $NdGaO_3$ taken at RT with $\lambda = 488$ nm and polarization along the principal crystal directions. Up to 16 peaks are resolved, most of them completely polarized; their frequencies and polarizations are listed in table 2. Since the xx spectrum is different from the yy we are certain that we are measuring a single-domain crystal with well defined OR axes. On the other hand, the $x'x'$ and $y'y'$ spectra are coincident, as they should be according to the tensors given above for pseudocubic axes.

Table 2. Frequency, polarization and symmetry assignment of $LaGaO_3$ and $NdGaO_3$ Raman modes observed in the orthorhombic phase (295 K). (x, y, z) and $(x', y', z' = z)$ stand for orthorhombic and pseudocubic axes respectively.

Frequency (cm^{-1})	Polarization	Symmetry
$LaGaO_3$ 57	xx, $x'x'$	A_g
92	$x'z$	B_{3g}
103	xy, $x'x'$	B_{1g}
118.5	xy, $x'x'$	B_{1g}
138	zz	A_g
143	$x'z$	B_{2g}
148	xy, $x'x'$	B_{1g}
173	xx, yy, zz, $x'x'$	A_g
177	$x'z$	B_{2g}
255	yy, zz	A_g
278	xx, zz, $x'x'$	A_g
336	$x'z$	B_{2g}
359	$x'x'$, xy, $x'z$	B_{1g}
434.5	$x'z$	$B_{2g} + B_{3g}$
450	zz, $x'x'$	A_g
$NdGaO_3$ 95	xx, yy, $x'x'$, $y'y'$, $x'y'$	A_g
142	yz	B_{3g}
144	xx, zz, xz, $x'x'$, $y'y'$, $x'y'$	A_g
151	xy, $x'x'$, $y'y'$	B_{1g}
168	xz	B_{2g}
199	xz, yz	$B_{2g} + B_{3g}$
212.5	xy, $x'x'$, $y'y'$	B_{1g}
214	zz, $x'x'$, $x'y'$, $y'y'$	A_g
289	yy, zz, yz, $x'x'$, $y'y'$, $x'y'$	A_g
336	xx, yy, $x'x'$, $y'y'$, $x'y'$	A_g
349	xz	B_{2g}
361.5	xy, $x'x'$, $y'y'$	B_{1g}
448	xy, $x'x'$, $y'y'$	B_{1g}
459	yz	B_{3g}
461	xz	B_{2g}
469	xx, yy, $x'x'$, $x'y'$	A_g

In figures 3(a) and 3(b) we present the RT Raman spectra of an $LaGaO_3$ single crystal in several polarizations and that of an $LaGaO_3$ ceramic sample. Up to 15 well resolved Raman peaks can be distinguished here. Due to the small crystal size we could only access the (001) and (110) OR planes. We have measured xx, yy, zz, xy, $x'x'$ and $x'z$ spectra. Though the OR directions could be identified by means of x-ray diffraction, we could not assign x and y axes unambiguously. Then, although the xx and yy spectra were found to be different, they could equally correspond to yy and xx configurations. Due to the presence of Nd^{3+} ions in the $LaGaO_3$ crystal, measurements were taken with the 514.5 and 457.9 nm Ar^+ lines to obtain a complete picture of the Raman spectra below 700 cm^{-1}. The mode

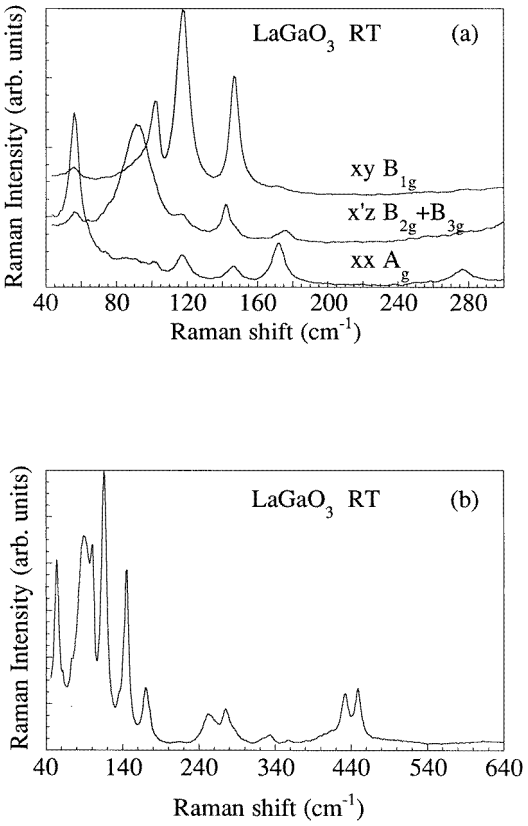

Figure 3. (a) RT Raman spectra of a 1% Nd doped $LaGaO_3$ single crystal with $\lambda = 514.5$ nm. x, y, z represent orthorhombic axes (x, y can be interchanged as y, x) and x' a cubic axis at approximately 45° between x, y. In this sample and with this laser line, strong Nd^{3+} emissions appear above 300 cm^{-1}. (b) RT Raman spectrum of an $LaGaO_3$ polycrystalline sample.

frequencies and polarizations are given in table 2. The presence of well polarized Raman peaks also corroborates the good orientation of the sample and that we had selected with the microscope a single domain.

The Raman frequencies of $NdGaO_3$ given in table 2 are very close to those found by Saine *et al* [11] in polycrystalline samples. However, they interpreted their spectrum in terms of the $Pbn2_1$ group, that predicts a much higher number of Raman active modes (57) than observed. The inconsistency, already noted by the authors of that work on comparing Raman and IR spectra, is wholly explained if the centrosymmetric $Pbnm$ group is assumed for $NdGaO_3$, as proposed in [3] by Marti *et al* and corroborated by us in section 3.

The assignment given in table 2 has been made with the use of the tensors expressed above. For the 144 and 289 cm^{-1} A_g modes some intensity is observed in forbidden configurations, probably due to a polarization leakage from the strong parallel components.

Since a and b axes could not be distinguished in orthorhombic $LaGaO_3$ we could not differentiate between B_{2g} and B_{3g} modes. This ambiguity has been solved by searching for a continuity in the mode assignment between the end compounds across the whole solid solution range. As for $NdGaO_3$ the detection of some modes with weak intensity in forbidden polarizations is attributed to polarization leakage or imperfect crystal orientation.

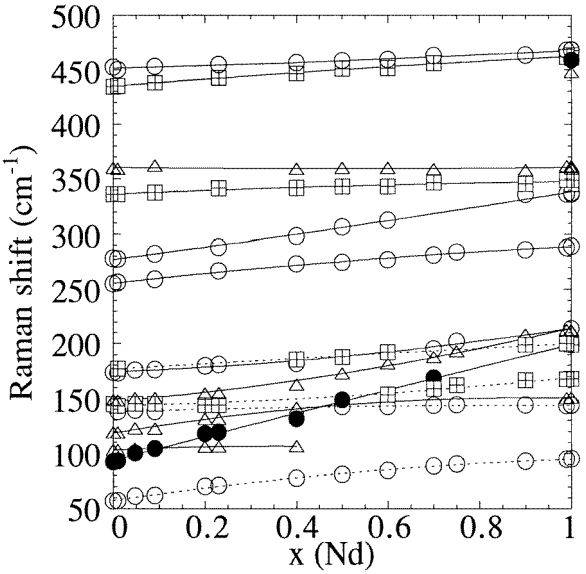

Figure 4. Raman frequencies against Nd concentration, x, of $La_{1-x}Nd_xGaO_3$ solid solutions. The symbols stand for the symmetry assignment as follows: ○ A_g, △ B_{1g}, ⊞ B_{2g}, ● B_{3g}. Dashed and continuous lines are only guides for the eye.

4.2. $La_{1-x}Nd_xGaO_3$ polycrystals, OR phase

The Raman spectra of $La_{1-x}Nd_xGaO_3$ polycrystalline samples have been measured at RT for 14 different compositions. Most of the modes detected in the single crystals are also seen in the ceramics and can be followed through the whole x range. Figure 4 shows the dependence of mode frequencies on composition. Except for some particular peaks, there is a general upward shift of the Raman frequencies with increasing Nd content, which is attributed to the lattice contraction upon replacement of La^{3+} by the smaller ion Nd^{3+}. Due to the continuous behaviour of the Raman spectrum as x varies, the mode symmetry at intermediate compositions can be inferred from the single crystal polarized spectra of the end compounds. Combining the results of $NdGaO_3$ and $LaGaO_3$ we obtain an assignment for 19 of the 24 Raman active modes expected for *Pbnm* space group for both pure compounds and their solid solutions.

In the 90 to 220 cm^{-1} region and for intermediate x values anticrossing effects between modes of the same symmetry are seen. This is particularly clear for B_{1g} symmetry, in complete analogy with the results in aluminates [16].

4.3. High temperature Raman spectra

The Raman spectra of $LaGaO_3$ and $NdGaO_3$ single crystals and of $La_{1-x}Nd_xGaO_3$ polycrystalline samples have been measured from 300 to 860 K. For $NdGaO_3$ single crystals we only observe the usual slight softening of the mode frequencies accompanied by line broadening as temperature increases.

In contrast, drastic changes occur in the Raman spectrum of $LaGaO_3$ around $T_c^{(1)} =$ 423 K, the temperature of the first order phase transition from OR to RH structure (see figure 5). The spectrum simplifies considerably and only four bands are observed above T_c. A remarkable feature is the large intensity increase of the lowest energy band in the high

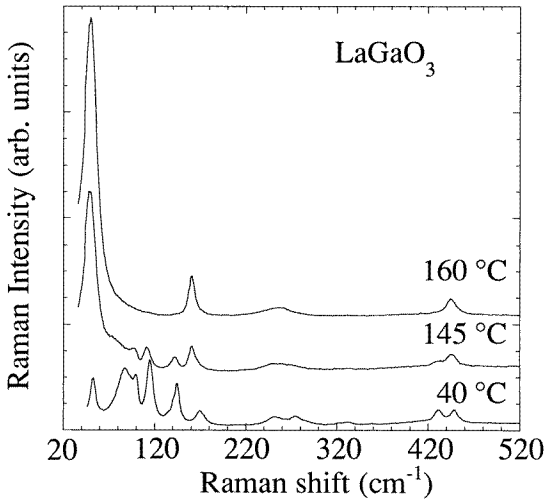

Figure 5. Raman spectrum of $LaGaO_3$ across the first order phase transition ($T_c^{(1)} \approx 150\,^{\circ}$C).

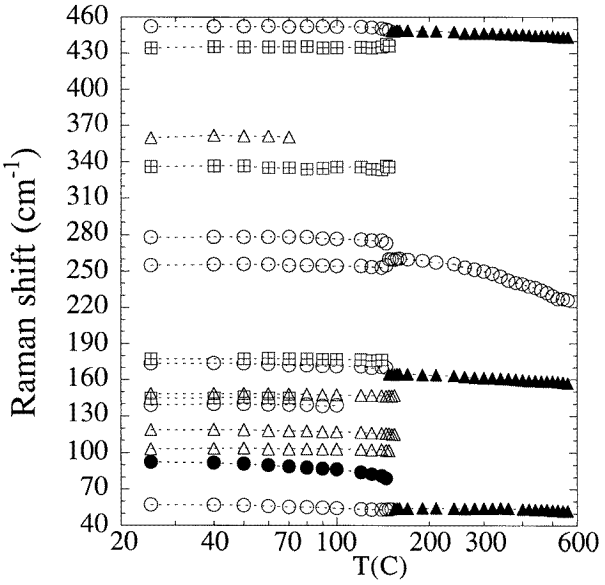

Figure 6. Temperature evolution of the Raman frequencies of $LaGaO_3$. Below T_c the symbols have the same meaning as in figure 4. Above T_c circles and triangles represent A_{1g} and E_g modes, respectively. Note the logarithmic scale on the temperature axis.

temperature phase. In figure 6 we plot the Raman frequencies as a function of temperature. We shall first describe the spectrum of $LaGaO_3$ at a fixed temperature above T_c and then its temperature evolution in the OR and RH phases separately.

4.3.1. $LaGaO_3$, RH phase. According to the more recent interpretation of Marti *et al* [3] the space group of the high temperature phase is the same as that of trigonal rare earth

Table 3. Frequency, symmetry assignment, atomic displacements and origin in cubic symmetry of Raman modes observed in the rhombohedral phase of $LaGaO_3$ ($T = 433$ K). The notation of the second column is the same as in the appendix.

Frequency (cm^{-1})	Symmetry and assignment	Origin in cubic phase
252	A_{1g}(O) (oxygen octahedron tilt)	R_{25}
52	E_g1(O) (oxygen octahedron tilt)	R_{25}
160	$E_g3(O) + E_g$(La) (in-plane La and O shifts)	$2R_{15}$
444	E_g2(O) (mainly La–O stretching)	R'_{12}

aluminates, i.e. the centrosymmetric $R\bar{3}c$ group. Since the unit cell contains two formula units ($Z = 2$), 30 lattice modes are expected. In this structure the rare earth occupies the 2b sites, gallium the inversion point site 2a and oxygen atoms the 6e sites, resulting in the following lattice modes at the zone centre:

$$\text{Ga: } A_{1u} + A_{2u} + 2E_u$$

$$\text{La: } A_{2g} + E_g + A_{2u} + E_u$$

$$\text{O: } A_{1g} + 2A_{2g} + 3E_g + A_{1u} + 2A_{2u} + 3E_u$$

five of which are Raman active: $A_{1g}(O) + 4E_g(La, O)$.

The Raman tensors for trigonal symmetry are usually referred to a set of orthogonal axes (x, y, z) such that z is along the trigonal axis (a pseudocubic [111] direction) and (x, y) lie in a plane perpendicular to z, instead of the RH ones, that form angles of 60°. These tensors are

$$\underset{A_{1g}}{\begin{bmatrix} a & & \\ & a & \\ & & b \end{bmatrix}}, \underset{E_g}{\begin{bmatrix} c & & \\ & -c & d \\ & d & \end{bmatrix}}, \underset{E_g}{\begin{bmatrix} & -c & -d \\ -c & & \\ -d & & \end{bmatrix}}.$$

Four bands can be seen in the high temperature phase of $LaGaO_3$. At 160 °C these are three relatively narrow ones at 52, 160 and 444 cm^{-1} and a broad one at 252 cm^{-1}. Polarization measurements performed in the single crystal indicate that the band at 252 cm^{-1} is the A_{1g} mode while the other three have E_g character (see table 3). There is, therefore, one missing E_g mode. We note that, if the space group were $R3c$, as previously proposed, a much greater number of Raman active modes (13) would be expected.

Since there are only a few Raman modes in the RH phase we can try to assign them from symmetry and energetic arguments. For this purpose we have worked out the normal displacements allowed by symmetry in the $R\bar{3}c$ group of $LaGaO_3$. These are given in hexagonal coordinates in the appendix. It is easy to see that A_{1g} and E_g1(O) modes correspond to the tilting of the GaO_6 octahedron around pseudocubic [111] and ([10$\bar{1}$], [01$\bar{1}$]) axes respectively, while E_g2(O), E_g3(O) and E_g(La) involve displacements of La and O atoms within the hexagonal ab plane.

We identify the rotational A_{1g} mode with the band of the same symmetry observed at 252 cm^{-1}. The assignment of the E_g modes is not so clear since O and La displacements allowed by symmetry can be mixed and, moreover, one of the E_g modes is not observed. The assignment given in table 3 has been made by relating the experimental frequency values with the atomic displacements allowed by symmetry, applying the correlation between cubic and RH space groups and also by making use of the strong similarities between the spectra of $LaGaO_3$ and those of trigonal aluminates [17–19]. In particular, the assignment of the 52 cm^{-1} mode to the oxygen cage rotation is based on the comparison with the analogous mode in $LaAlO_3$ and its soft mode character (see section 4.3.3).

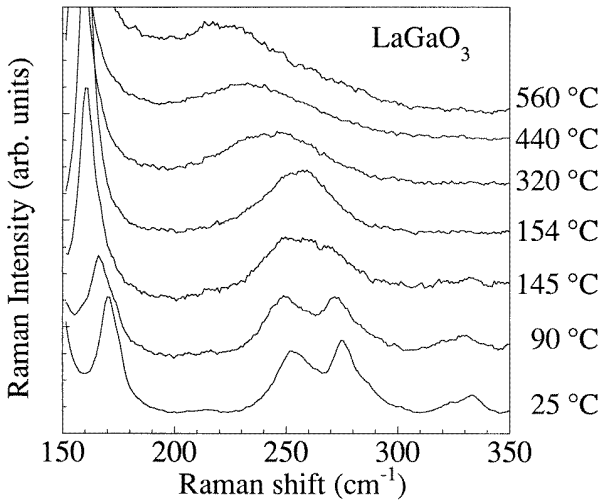

Figure 7. Temperature evolution of the Raman spectrum of $LaGaO_3$ in the region of the totally symmetric soft mode (≈250 cm^{-1}).

4.3.2. Temperature evolution from RT to $T_c^{(1)}$ (OR phase). The most remarkable feature in this region is softening of the 92 cm^{-1} (B_{3g}) mode at temperatures close to $T_c^{(1)} = 423$ K. A more complex behaviour is observed in doped compounds. In the $x = 4.75\%$ sample, for instance, where $T_c^{(1)}$ has increased up to 513 K (thus allowing us to follow the OR modes much further than in $LaGaO_3$) softening is remarkable for the B_{3g} mode (99 cm^{-1} at RT) and also for the low frequency A_g mode (60 cm^{-1} at RT). Since the OR to RH phase transition is of abrupt first order character no soft modes are expected, so that this behaviour must have another explanation. At this point, a correlation between modes in OR and RH phases with those of the ideal cubic structure can be useful.

As discussed in the introduction, RH and OR phases can be viewed as the result of condensation of zone edge lattice modes of the cubic structure $Pm3m$, specifically R_{25} (out-of-phase octahedron rotation) for the RH phase and mainly R_{25} plus M_3 (in-phase rotation) for the OR phase [20]. The cubic R_{25} mode splits as $A_{1g} + E_g$ in the RH phase and as $A_g + B_{1g} + B_{3g}$ in the OR phase. In section 4.3.1 we have attributed the A_{1g} and E_g modes corresponding to octahedron tilts in the RH phase to bands observed at 252 and 52 cm^{-1}, respectively, in $LaGaO_3$. If the A_{1g} is correlated to an OR A_g mode (and there are no other possibilities in that frequency region) the *rotational* E_g mode must correspond to a pair $B_{1g} + B_{3g}$ in the OR phase. We identify the B_{3g} component with the mode at 92 cm^{-1}. Then, in spite of the frequency coincidence and softening properties, the low frequency OR A_g mode cannot be a component of the rotational E_g mode. On the other hand, the cubic M_3 mode transforms as A_g in the OR phase and is a good candidate to be the lowest A_g mode. The softening of A_g and B_{3g} modes, also seen in OR aluminates $SmAlO_3$ and $EuAlO_3$ [8, 9], would be a trace of the intrinsic tendency of the OR structure toward cubic symmetry, truncated by the phase transition to the RH phase.

4.3.3. Temperature evolution above $T_c^{(1)}$ (RH phase). In this phase only the A_{1g} mode shows and anomalous behaviour, softening and broadening remarkably with increasing temperature, as can be seen in the expanded spectra of figure 7. This behaviour is similar, though less pronounced, to that of the corresponding A_{1g} mode in trigonal $LaAlO_3$ when approaching

the second order phase transition to cubic symmetry [17], and supports the assignment of the A_{1g} mode in $LaGaO_3$ to the GaO_6 octahedron rotation around a [111] pseudocubic axis. The low frequency E_g mode involves, as the A_{1g}, tilting of the GaO_6 octahedron, and is also expected to soften with increasing temperature, but the slight downshift of all the E_g modes observed experimentally is unmeaningful.

The observation of a soft A_{1g} mode in the RH phase of $LaGaO_3$ is a hint of a hypothetical (not found at least up to 1673 K [2]) second order phase transition from RH to cubic symmetry, analogous to that of RH aluminates $LaAlO_3$, $PrAlO_3$ and $NdAlO_3$. These three compounds have the $R\bar{3}c$ structure at RT and transform to the cubic perovskite phase with increasing values of $T_c^{(2)}$ (800 K for La, 1640 K for Pr and 2020 K for Nd), as corresponds to increasing magnitude of trigonal distortion. The distortion can be measured, for instance, by the departure of the c/a ratio from the value ($\sqrt{6}$) in perfect cubic symmetry, c and a being hexagonal lattice parameters: c/a is 2.444 for $LaAlO_3$ [7], 2.432 for $PrAlO_3$ [7] and 2.427 for $NdAlO_3$ [5], all at RT, and 2.421 for $LaGaO_3$ at 300 °C [3]. An extrapolation of the T_c–c/a dependence gives $T_c^{(2)} > 2200$ K for $LaGaO_3$, well above its melting temperature. Therefore, the RH to cubic phase transition is unobservable in $LaGaO_3$.

The much higher transition temperature of $LaGaO_3$ as compared with $LaAlO_3$ explains the absence of softening in the low frequency E_g and the weaker softening of the A_{1g} mode. We note that, from trigonal aluminates, $LaAlO_3$ is the only one that shows a soft E_g mode, specifically the low frequency one, which has meant its attribution to the rotation of oxygen octahedra arising, as the A_{1g}, from the R_{25} mode that condenses at $T_c^{(2)}$ to give the RH symmetry [17].

The assignment of A_{1g} and E_g soft modes to peaks at 252 and 52 cm^{-1} allows us to use the Thomas–Müller theory [21] to analyse the results. According to this model, which applies to second order phase transitions driven by the rotational R_{25} mode, the frequencies of the soft modes in the low temperature phase, ω_E and ω_A, are related to the coefficients of the quartic terms of the anharmonic potential, b and c, as $\omega_E^2/\omega_A^2 = (b-c)/(b+2c)$. With the values of ω_E and ω_A given above we obtain $b \approx 1.13c$, close to the result for trigonal aluminates and within the region of stability of the RH phase ($b > c$, $b+2c > 0$).

5. The first order phase transition as a function of Nd concentration

In figure 8 we show the first order transition temperature $T_c^{(1)}$ as a function of x. For small x $(0, 0.01)$ a well defined phase transition is found, in the sense that we observe in a small temperature range (about five degrees) the disappearance of the OR spectrum and the appearance of the RH one, whose most remarkable signature is the huge increase of the 52 cm^{-1} mode. For greater x $(0.05, 0.09, 0.14)$ the OR spectrum persists over 20 to 30 degrees superposed to the RH spectrum until it disappears. Finally, for the last sample studied, with $x = 0.2$, no trigonal spectrum could be found up to 860 K, though the OR spectrum suffers strong intensity and linewidth changes and a broad background develops from about 190 cm^{-1} towards the laser line.

Raman results on the phase transition are in agreement with DSC measurements, that indicate a first order transition with critical temperature increasing and enthalpy change ΔH decreasing as x increases. For $x \geqslant 0.1$ ΔH is so small that the peak is not resolved from the equipment background signal.

The $T_c^{(1)}$–x data can be fitted to the following quadratic expression

$$T_c = 424.5 + 1670.5x + 5562.4x^2.$$

Extrapolated to $x = 0.2$ this line predicts a phase transition at about 980 K, above the upper limit of our measurements. For $x = 0.4$ it gives 1983 K, close to the melting temperatures of

these compounds. Then, it can be concluded that the presence of increasing amounts of Nd hinders the OR to RH transition. Since $NdGaO_3$ does not show the phase transition at all it is not surprising that there is a partial Nd/La substitution at which the phase transition is lost. The case is contemplated in the work of Mitra [22] for second order transitions, but it may of interest to recall it here, at least qualitatively. Within this model and considering $NdGaO_3$ as a compound having infinite T_c, it is expected that there is a critical Nd concentration in the solid solution above which the phase transition does not occur below the melting temperature.

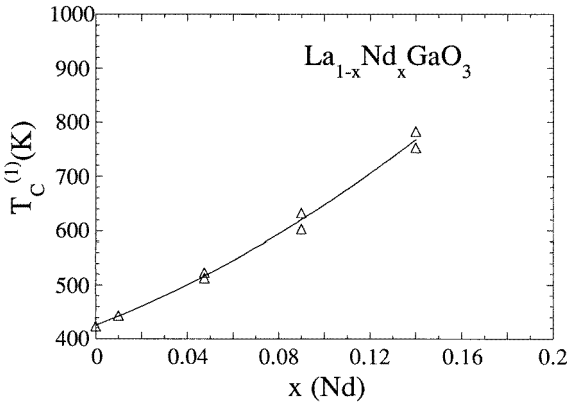

Figure 8. Critical temperature of the first order phase transition ($Pbnm \rightarrow R\bar{3}c$) as a function of Nd content, x. The continuous line is the fit to a quadratic dependence, as given in the text. Two T_c values at a fixed x indicate the interval of coexistence of OR and RH spectra.

Another point that is worth mentioning is that $T_c^{(1)}$ increases on going towards more compressed lattices (increasing x). This is the usual behaviour in a zone edge boundary phase transition of second order [23]. The arguments given in that reference seem to be valid in our case though the transition is of first order.

Qualitatively, the OR–RH phase stability can be discussed in terms of tolerance factors or similar parameters reflecting the presence of internal strains in the perovskite structure at low temperature [24]. In $LaGaO_3$ the Ga–O bond is slightly compressed while the La–O bond is extended with respect to their equilibrium distances (taken, for instance, as the sum of ionic radii). This corresponds to type II (tilting region) of the Kassan–Ogly classification of perovskite loose packing [24], in contrast with rare earth aluminates, where the strain of A–O and B–O bonds is smaller and belongs to region III. The introduction of substitutional Nd ions in $LaGaO_3$, with the subsequent cell parameter and effective rare earth radius reduction, increases the internal strain in both types of bond and the OR structure is stabilized against the RH one. This is reflected (see table 1) in the increasing shift of rare earth atoms from their ideal cubic positions or in the decrease of Ga–O–Ga angles, indicating stronger octahedron tilts with increasing value of x. We also note that octahedra tilts preserve the Ga–O6 coordination, with small variations of Ga–O bond lengths. In contrast, the rare earth environment is strongly affected. Some of the rare earth–O distances decrease while others increase, resulting in a lower coordination number for the rare earth in $NdGaO_3$ than in $LaGaO_3$.

The apparent coexistence of OR and RH spectra in a temperature interval around T_c increasing with x can have several explanations: temperature or x inhomogeneity, or intrinsic reasons. The first one could be due to local heating by the laser beam producing a

temperature gradient in the sample. However, this is expected to affect all samples in the same manner, irrespective of x. The other possibility is that the Nd content varies slightly among the grains composing the sample. Considering the pronounced $T_c(x)$ dependence, a fluctuation of about 10% over nominal x value is enough to produce the interval in T_c. This distribution of x values would also explain the larger width of the Raman peaks in polycrystalline samples with $x \neq 0$. A final possibility is that this is a deeper physical phenomenon and that there is a distribution in T_c values even for a well defined Nd concentration, as a result of disorder or local Nd distribution. These arguments are similar to those proposing the formation of precursor clusters having the low temperature phase above the critical temperature in first order phase transitions [25], though in our case they would be due to Nd inhomogeneous distribution and not to fluctuations. On the other hand, this is in contradiction with the general observation that the effect of dilution between isomorphous compounds is homogeneous throughout the crystal so that a single critical temperature is found [22]. More experimentation, such as high temperature XRD in single crystals of mixed composition, would be needed to clarify this point.

6. Summary and conclusions

We have studied the $La_{1-x}Nd_xGaO_3$ system by means of Raman and x-ray diffraction. Both techniques confirm that $LaGaO_3$ and $NdGaO_3$ present the $Pbnm$ space group at RT. The same symmetry is found for intermediate compositions in the whole solid solution range. Our results also confirm the $R\bar{3}c$ space group for the high temperature phase of $LaGaO_3$. Polarization measurements in single crystals have allowed us to assign the symmetry of all modes observed. In the RH phase we have been able to identify the atomic displacements involved in each mode.

The first order phase transition form OR to RH symmetry has been studied in $LaGaO_3$ and compounds with small Nd content through the temperature evolution of Raman spectra. The critical temperature $T_c^{(1)}$ is found to increase quadratically with x in the region $0 \leqslant x < 0.2$ measured.

Soft modes are found both in OR and in RH phases. This behaviour is discussed within usual models for phase transitions in perovskites. The detection of a soft A_{1g} mode in the RH phase of $LaGaO_3$, in particular, is interpreted as indication of a phase transition from RH to cubic symmetry, predicted at temperatures above the melting point.

Rare earth gallates and aluminates present remarkable similarities, not only of structural type: their Raman spectra show a very similar mode pattern, temperature evolution and composition dependence upon rare earth substitution. This common behaviour has been useful in mode attribution and also supports our hypothesis that a virtual (unreachable) phase transition to cubic symmetry exists in $LaGaO_3$.

From our work a proposal can be made concerning the possible technological application of the strong $T_c(x)$ dependence in the use of these materials as substrates. A slightly doped compound of the $La_{1-x}Nd_xGaO_3$ series would have intermediate matching conditions with $T_c^{(1)}$ much higher than in $LaGaO_3$ and smaller microwave absorption than in $NdGaO_3$, if x is adequately chosen.

Acknowledgments

We appreciate the contribution of Inés García Rubio to the production of samples, the participation of María Angeles Laguna in Raman measurements of $NdGaO_3$ and the technical

support of Rosa García Casanova in DSC measurements. The work has been done with financial support from CICYT under contract MAT97-0673-C02-01.

Appendix

Displacements allowed by symmetry in Raman active modes of ABO_3 perovskites in rhombohedral phase (space group $R\bar{3}c$). (x, y, z) represent hexagonal axes, with $z \parallel$ trigonal axis and x, y in a perpendicular plane, forming an angle of 120°. The labelling of the oxygen and A (La) atoms corresponds to that of figure A1. A given oxygen octahedron can be formed by taking the two triangles (O1, O2, O3) and (O4, O5, O6) as (111) pseudocubic faces.

$$
\begin{aligned}
&A_{1g}: \quad O1y + O2x - O3(x+y) + O4(x+y) - O5x - O6y\\
&E_g1(O): -O1z + 2O2z - O3z + O4z - 2O5z + O6z\\
&\qquad -O1z - O2z + 2O3z - 2O4z + O5z + O6z\\
&E_g2(O): -O1y + 2O2x + O3(x+y) - O4(x+y) - 2O5x + O6y\\
&\qquad 2O1y - O2x + O3(x+y) - O4(x+y) + O5x - 2O6y\\
&E_g3(O): O1(x+y) + 2O2y - O3x + O4x - 2O5y - O6(x+y)\\
&\qquad 2O1x + O2(x+y) - O3y + O4y - O5(x+y) - 2O6x\\
&E_g(La): La1x - La2x\\
&\qquad La1y - La2y.
\end{aligned}
$$

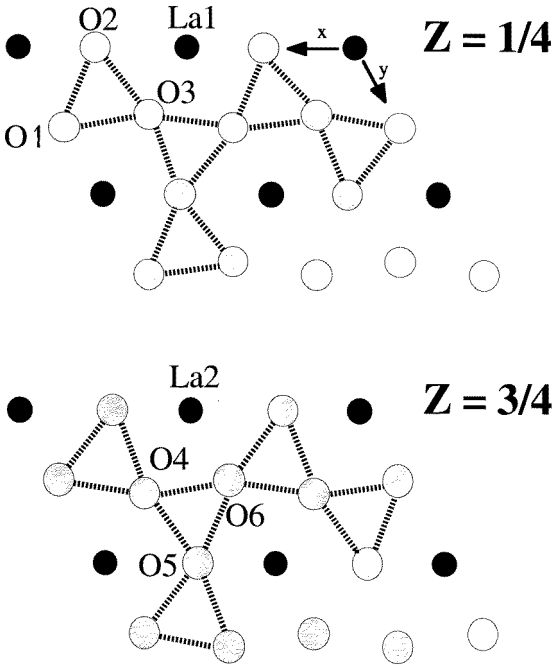

Figure A1. $z = 1/4$ and $z = 3/4$ hexagonal planes of $LaGaO_3$ perovskite in the rhombohedral phase. x and y hexagonal axes are taken along $[10\bar{1}]$ and $[\bar{1}10]$ pseudocubic axes, while z is along the [111] pseudocubic axis.

References

[1] Phillips J M 1996 *J. Appl. Phys.* **79** 1829–48
[2] Marti W, Fischer P, Altorfer F, Scheel H J and Tadin M 1994 *J. Phys.: Condens. Matter* **6** 127–35
[3] Marti W, Fischer P, Schefer J and Kubel F 1996 *Z. Kristallogr.* **211** 891–4
[4] Derighetti B, Drumheller J E, Laves F, Müller K A and Waldner F 1965 *Acta Crystallogr.* **18** 557
[5] Marezio M, Dernier P D and Remeika J P 1972 *J. Solid State Chem.* **4** 11–19
[6] Hellwege K H ed 1970 *Landolt–Börnstein New Series* vol 4a (Berlin: Springer)
[7] Geller S and Raccah P M 1970 *Phys. Rev.* B **2** 1167–72
[8] Alain P and Piriou B 1975 *Rev. Int. Hautes Temp. Réfract.* **12** 35–9
[9] Alain P and Piriou B 1975 *Solid State Commun.* **17** 35–9
[10] Glazer A M 1972 *Acta Crystallogr.* B **28** 3384
Glazer A M 1975 *Acta Crystallogr.* A **31** 756
[11] Saine M C, Husson E and Brusset H 1982 *Spectrochim. Acta* **38** 19–24
[12] Rodríguez-Carvajal 1993 *Physica* B **192** 55
[13] Shannon R D 1976 *Acta Crystallogr.* A **32** 751
[14] Brown I D and Shannon R D 1973 *Acta Crystallogr.* A **29** 266
[15] Some confusion is frequently found in the labelling of the modes due to the election of OR axes. The decomposition given above corresponds to *Pbnm* group, while those pertaining to *Pnma* are usually found in the tables.
[16] Alain P and Piriou B 1977 *J. Physique.* **38** C7 389
[17] Scott J F 1969 *Phys. Rev.* **183** 823–5
[18] Harley R T, Hayes W, Perry A M and Smith S R P 1973 *J. Phys. C: Solid State Phys.* **6** 2382–400
[19] Finkmann E, Cohen E and Van Uitert L G 1973 *Phys. Rev.* B **7** 2899
[20] Participation of other modes is allowed by symmetry in the OR case but will not be considered here. The origin is taken at atom A of the perovskite structure. If the origin is taken at atom B R_{25} and M_3 modes are labelled as R'_{15} and M_2, respectively.
[21] Thomas H and Müller K A 1968 *Phys. Rev. Lett.* **21** 1256
[22] Mitra S S 1982 *J. Phys. C: Solid State Phys.* **15** 453–62
[23] Samara G A, Sakudo T and Yoshimitsu K 1975 *Phys. Rev. Lett.* **35** 1767–79
[24] Kassan-Ogly F A and Naish V E 1986 *Acta Crystallogr.* B **42** 307–13
Kassan-Ogly F A and Naish V E 1986 *Acta Crystalogry.* B **42** 325–35
[25] Cook H E 1977 *Phys. Rev.* B **15** 1477–88